

Controlling the s -wave scattering length with nonresonant light: Predictions of an asymptotic model

Anne Crubellier,^{1,*} Rosario González-Férez,^{2,†} Christiane P. Koch,^{3,‡} and Eliane Luc-Koenig^{1,§}

¹Laboratoire Aimé Cotton, UMR No. 9188, CNRS, Université Paris–Sud, Université Paris–Saclay, ENS Cachan, Faculté des Sciences d’Orsay, Bâtiment 505, 91405 Orsay Cedex, France

²Instituto Carlos I de Física Teórica y Computacional and Departamento de Física Atómica, Molecular y Nuclear, Universidad de Granada, 18071 Granada, Spain

³Theoretische Physik, Universität Kassel, Heinrich-Plett-Straße 40, 34132 Kassel, Germany

(Received 22 November 2016; published 8 February 2017)

A pair of atoms interacts with nonresonant light via its anisotropic polarizability. This effect can be used to tune the scattering properties of the atoms. Although the light-atom interaction varies with interatomic separation as $1/R^3$, the effective s -wave potential decreases more rapidly as $1/R^4$ such that the field-dressed scattering length can be determined without any formal difficulty. The scattering dynamics are essentially governed by the long-range part of the interatomic interaction and can thus be accurately described by an asymptotic model [A. Crubellier *et al.*, *New J. Phys.* **17**, 045020 (2015)]. Here we use the asymptotic model to determine the field-dressed scattering length from the s -wave radial component of a particular threshold wave function. Applying our theory to the scattering of two strontium isotopes, we calculate the variation of the scattering length with the intensity of the nonresonant light. Moreover, we predict the intensities at which the scattering length becomes infinite for any pair of atoms.

DOI: [10.1103/PhysRevA.95.023405](https://doi.org/10.1103/PhysRevA.95.023405)

I. INTRODUCTION

Collisions of neutral atoms at very low temperatures are universally described by a single parameter, the s -wave scattering length for bosons and unpolarized fermions or the p -wave scattering volume for polarized fermions. These parameters determine the strength of the contact potentials for all partial waves [1,2]. Their values determine whether an ultracold gas is weakly or strongly interacting and their sign renders the interaction to be effectively attractive or repulsive [3]. This is important, for example, for the stability of Bose-Einstein condensation or the stability of Fermi gases against collapse at high densities. Controlling the scattering length or the scattering volume therefore has long been a primary goal in quantum gas experiments [4–9].

While initial proposals suggested optical means for control [10–13], tuning the scattering length using a magnetic field and Feshbach resonances turned out to be more practical [4,5]. This requires, however, the existence of a hyperfine manifold on the atom and a sufficient width of the Feshbach resonance. In contrast, optical control of the scattering length is ubiquitous. It was demonstrated for narrow-line transitions that are found, for example, in alkaline-earth atoms [7–9]. Despite the comparatively long lifetimes of the metastable states employed in these experiments, control was limited by non-negligible losses.

Nonresonant light can also be used to tune the scattering length [14,15]. It couples to the polarizability anisotropy of the collision complex and, for sufficiently high intensity, modifies the scattering length [15]. This variation is similar to the

control of the scattering length by a magnetic field near a Feshbach resonance [5]. In particular, the scattering length diverges when a bound level is located exactly at threshold. For nonresonant light control this occurs when a shape resonance crosses the threshold to become bound or when the field-dressed s -wave potential is sufficiently deepened to accommodate an additional bound level. Remarkably, nonresonant light control is of universal character, independent of the frequency of the light and the energy-level structure of the molecule, as long as the frequency remains far from any molecular resonance [14,15].

Collisions at very low temperature are essentially governed by the long-range part of the interparticle interaction. The scattering properties are therefore very well described by asymptotic models, which account only for the asymptotic part of the interaction potential [16–23]. The asymptotic Hamiltonian describing nonresonant light control of a pair of atoms [22,23] is identical to that found for dc electric field control of the atom-atom interaction [24] as well as that for ultracold collisions of polar molecules [25,26]. All of these problems are governed by the anisotropic dipole-dipole interaction, which decreases as $1/R^3$ (where R is the interparticle separation) and introduces a coupling between partial waves of the same parity.

For an isotropic potential that decreases asymptotically as $1/R^3$, it is well known that the scattering length cannot be defined [27]. In this case, the scattering phase shift at low energy cannot be expanded in powers of the wave number of the colliding particles since the threshold wave function contains a $\log R$ contribution in addition to the term proportional to $R - \tilde{a}$ that is used to define the scattering length \tilde{a} . However, the dipole-dipole interaction is anisotropic and only of quasi-long-range character [24], which allows us to define the scattering length without any particular difficulty. Quasi-long-range refers to the fact that the effective s -wave potential decreases as $1/R^4$ for large R and only the potential

*anne.crubellier@u-psud.fr

†rogonzal@ugr.es

‡christiane.koch@uni-kassel.de

§eliane.luc@u-psud.fr

for the higher partial waves contains a diagonal long-range contribution proportional to $-1/R^3$ [28].

Here we investigate nonresonant light control of the scattering length. We show that the asymptotic model together with the nodal line technique [29,30], previously developed to study nonresonant light control of shape resonances [22,23], can be extended to the control of the field-dressed s -wave scattering length \tilde{a} . To predict the dependence of the field-dressed scattering length on the nonresonant field intensity, the asymptotic model only requires knowledge of the reduced mass, atomic polarizability, and field-free s -wave scattering length. The difficulty that we have to address here is the problem of degenerate coupled continua. We obtain \tilde{a} from a particular threshold wave function that has a linear variation in the $\ell = 0$ partial wave channel and does not diverge in all others.

The paper is organized as follows. In Sec. II we review the asymptotic model for an atom pair interacting with nonresonant light via the polarizability anisotropy [22]. We present the Hamiltonian in two types of reduced units, best adapted to either the nonresonant field control or the dipole-dipole interaction. In Sec. III we describe the method to calculate scattering wave functions. In particular, in Sec. III B we discuss the asymptotic form imposed on the degenerate threshold wave functions. It is a judicious choice of this form that allows for determining the scattering length. For more details of the method, in particular an assessment of its validity and the optimal choice of the asymptotic boundary conditions, the reader is referred to the Appendix. The discussion is based on the comparison between single-channel analytical calculations based on an extension of the Levy-Keller approach [31] and additional multichannel numerical calculations. In Sec. IV we first apply our model to two strontium isotopes ^{88}Sr and ^{86}Sr and calculate the dependence of the intraspecies ^{88}Sr - ^{88}Sr and the interspecies ^{86}Sr - ^{88}Sr scattering lengths on the nonresonant light intensity. We then exploit the universality of ultracold collisions, captured by the asymptotic model, and predict the nonresonant light intensity at which the scattering length becomes infinite. We summarize in Sec. V.

II. LENGTH AND ENERGY SCALES FOR ANISOTROPIC R^{-3} INTERACTION: HAMILTONIAN AND REDUCED UNITS

In the Born-Oppenheimer approximation, the Hamiltonian describing the nuclear relative motion of a pair of atoms interacting with a nonresonant laser field is given by

$$H = T_R + \frac{\hbar^2 \mathbf{L}^2}{2\mu R^2} + V_g(R) - \frac{2\pi I}{c} [\Delta\alpha(R) \cos^2 \theta + \alpha_{\perp}(R)], \quad (1)$$

where T_R and $\hbar^2 \mathbf{L}^2 / 2\mu R^2$ are the vibrational and rotational kinetic energies, respectively, and μ denotes the reduced mass, R the interatomic separation, and $V_g(R)$ the interaction potential of the electronic ground state. The last term in the Hamiltonian (1) stands for the interaction with a nonresonant light field of intensity I , linearly polarized along the space-fixed Z axis. Here θ denotes the polar angle between the interatomic axis and the laser polarization axis and c the

velocity of light. The perpendicular and parallel components of the polarizability tensor, $\alpha_{\perp}(R)$ and $\alpha_{\parallel}(R)$, are defined with respect to the interatomic axis, and have the dimension of a volume [22]. The polarizability anisotropy is given by $\Delta\alpha(R) = \alpha_{\parallel}(R) - \alpha_{\perp}(R)$.

In the asymptotic approximation, $V_g(R)$ is replaced by the van der Waals interaction $-C_6/R^6$ and the molecular polarizabilities are expressed in terms of the polarizabilities of the two constituent atoms α_1 and α_2 as follows: $\alpha_{\parallel}(R) = \alpha_1 + \alpha_2 + 4\alpha_1\alpha_2/R^3$ and $\alpha_{\perp}(R) = \alpha_1 + \alpha_2 - 2\alpha_1\alpha_2/R^3$ [32–34]. The rovibrational Hamiltonian (1) then becomes

$$H = T_R + \frac{\hbar^2 \mathbf{L}^2}{2\mu R^2} - \frac{C_6}{R^6} - \frac{2\pi I}{c} \left((\alpha_1 + \alpha_2) + 2\alpha_1\alpha_2 \frac{3 \cos^2 \theta - 1}{R^3} \right). \quad (2)$$

In the second line, the term $E_0 = -2\pi I(\alpha_1 + \alpha_2)/c$ represents the lowering of the dissociation limit due to the interaction with the nonresonant field. The last term in the large parentheses is very similar to the one involved in dipole-dipole scattering in ultracold gases of atoms or molecules, with either permanent or field-induced dipole moments. This is not surprising since the polarizability coupling describes nothing but the interaction of the two dipoles induced by the nonresonant field. The correspondence between Eq. (2) and the standard dipole-dipole interaction for electric (magnetic) dipoles becomes obvious by writing

$$\frac{4\pi I}{c} \alpha_1 \alpha_2 \leftrightarrow \frac{1}{4\pi \epsilon_0} d_1 d_2 \leftrightarrow \frac{\mu_0}{4\pi} m_1 m_2, \quad (3)$$

where $d_{1,2}$ ($m_{1,2}$) denotes the magnitude of the electric (magnetic) dipole moments.

In the Hamiltonian (2), the van der Waals potential $V_g(R) = -C_6/R^6$ represents the short-range physics, which prevails when the atoms are rather close together but still in the asymptotic region, whereas the long-range dynamics is governed by the dipole-dipole interaction induced by the nonresonant field. Thus, two length and energy scales can be defined in the problem. The first one, well adapted to the interaction with a low-intensity nonresonant field, is independent of the field intensity and characteristic of the short-range interaction. The other one is characteristic of the dipole-dipole interaction and allows us to highlight the universal character of the dipolar scattering.

Analogously to Ref. [22], we introduce reduced units (ru) [21] to treat the centrifugal term and the van der Waals interaction on an equal footing. The reduced units are $R = \sigma x$, $E - E_0 = \epsilon \mathcal{E}$, and $I = \beta \mathcal{I}$ for length, energy, and laser intensity, respectively, with

$$\sigma = \left(\frac{2\mu C_6}{\hbar^2} \right)^{1/4}, \quad (4a)$$

$$\epsilon = \frac{\hbar^2}{2\mu \sigma^2}, \quad (4b)$$

$$\beta = \frac{c}{12\pi} \frac{\hbar^{3/2} C_6^{1/4}}{\alpha_1 \alpha_2 (2\mu)^{3/4}} = \frac{c \sigma^3 \epsilon}{12\pi \alpha_1 \alpha_2}. \quad (4c)$$

These unit conversion factors contain information specific to the atom pair, i.e., the reduced mass μ , the van der Waals coefficient C_6 , and the atomic polarizabilities α_1 and α_2 . In reduced units, the asymptotic Schrödinger equation reads

$$\left[-\frac{d^2}{dx^2} - \frac{1}{x^6} + \frac{\mathbf{L}^2}{x^2} - \mathcal{I} \frac{\cos^2 \theta - 1/3}{x^3} - \mathcal{E} \right] f(x, \theta, \varphi) = 0, \quad (5)$$

where φ is the azimuthal angle and $f(x, \theta, \varphi)$ is the wave function in the asymptotic limit.

Following Ref. [26] and using the equivalent dipoles defined by the relations (3), we define a second set of reduced units $R = D\bar{x}$ and $E = E_D\bar{\mathcal{E}}$, characteristic of the dipole-dipole interaction and involving thus intensity-dependent conversion factors,

$$D = \frac{\mu}{\hbar^2} \frac{4\pi\alpha_1\alpha_2}{c} I, \quad (6a)$$

$$E_D = \frac{\hbar^2}{\mu D^2} = \frac{4\pi\alpha_1\alpha_2}{c} \frac{I}{D^3}. \quad (6b)$$

In these reduced units, the asymptotic Schrödinger equation reads

$$\left[-\frac{d^2}{d\bar{x}^2} - \frac{\bar{c}_6}{\bar{x}^6} + \frac{\mathbf{L}^2}{\bar{x}^2} - 6 \frac{\cos^2 \theta - 1/3}{\bar{x}^3} - 2\bar{\mathcal{E}} \right] f(\bar{x}, \theta, \varphi) = 0, \quad (7)$$

where \bar{c}_6 is the reduced strength of the van der Waals interaction

$$\bar{c}_6 = 2\mu C_6 / \hbar^2 D^4. \quad (8)$$

The two sets of reduced units are related as

$$D = \frac{\mathcal{I}}{6} \sigma, \quad (9a)$$

$$E_D = \frac{72}{\mathcal{I}^2} \epsilon. \quad (9b)$$

Whereas in Eq. (5) the short-range van der Waals interaction is described by a universal term, it is the long-range dipole-dipole interaction that appears as universal in Eq. (7). The nonuniversal parameters of the two equations, \bar{c}_6 and \mathcal{I} , are related by

$$\bar{c}_6 = \frac{\sigma^4}{D^4} = \frac{6^4}{\mathcal{I}^4}. \quad (10)$$

To give an example, the reduced units for $^{88}\text{Sr}_2$ are $\sigma = 151a_0$, $\epsilon = 86 \mu\text{K}$, and $\beta = 0.636 \text{ GW cm}^{-2}$ [22,23]. For nonresonant intensities $\mathcal{I} \leq 40 \text{ ru}$ (25 GW cm^{-2} for strontium), the ratio $D/\sigma \leq 6.6$ results in an intensity-dependent unit of length $D \leq 10^3 a_0$. For comparison, we will consider the heteronuclear dialkali-metal molecules with the smallest and the largest permanent electric dipole moment, which amount to 0.56 D (KRb) and 5.5 D (LiCs) [26,35]. For the dipole-dipole interaction between two KRb or two LiCs molecules, the reduced unit of length is very large, $D_{\text{KRb}} = 4800a_0$ or $D_{\text{LiCs}} = 6 \times 10^5 a_0$, while the reduced unit of energy is very small $E_{D,\text{KRb}} = 120 \text{ nK}$ or $E_{D,\text{LiCs}} = 7 \text{ pK}$. In order to observe, with strontium atoms in a nonresonant field, effects similar to those

encountered in the dipolar scattering of these polar molecules, an intensity-dependent unit of length D of the same order of magnitude is needed. This implies huge nonresonant field intensities, i.e., $\mathcal{I} \approx 100 \text{ ru}$ (65 GW cm^{-2}) would be required to obtain the same behavior as for KRb and $\mathcal{I} \approx 3500 \text{ ru}$ (2200 GW cm^{-2}) to mimic LiCs. The short-range van der Waals interaction between two dialkali-metal molecules in their absolute ground states is very small, with $\bar{c}_6 = 7 \times 10^{-6}$ or $9 \times 10^{-9} \text{ ru}$ for KRb or LiCs, respectively. In these systems, the long-range dipole-dipole interaction prevails, such that the van der Waals interaction can be neglected in Eq. (7), and the short-range physics is taken into account by including a repulsive wall [26]. This is in contrast to strontium where, for the nonresonant light intensity that we consider, the van der Waals term cannot be neglected.

III. ASYMPTOTIC MODEL AND NODAL LINE TECHNIQUE

A. General description of the method

To solve the asymptotic Schrödinger equation (5), we first expand the wave function $f(x, \theta, \varphi)$ in terms of spherical harmonics $Y_\ell^m(\theta, \varphi)$ with fixed magnetic quantum number m and the same parity, i.e., even or odd values of ℓ , due to the symmetry of the Hamiltonian (2). For practicality, the infinite sum over partial waves needs to be restricted to ℓ varying from $\ell_{\min} = |m|$ to ℓ_{\max} and includes $n = (\ell_{\max} - \ell_{\min} + 2)/2$ channels. Thus, a solution of Eq. (5) is given by

$$f(x, \theta, \varphi) = \sum_{\ell=\ell_{\min}}^{\ell_{\max}} y_\ell(x) Y_\ell^m(\theta, \varphi), \quad (11)$$

where the sum runs over either even or odd values of ℓ and $y_\ell(x) \equiv y_{\ell,m}(x)$ is the radial component of the solution in the channel ℓ , m . For simplicity, the magnetic quantum number m is not specified in the radial part of wave function $y_\ell(x)$. The amount of channels n that needs to be included in (11) depends on the energy and on the laser intensity.

This basis set expansion transforms the asymptotic Schrödinger equation (5) into the system of coupled equations

$$\frac{d^2}{dx^2} \mathbf{y}(x) + (\mathbf{M} + \mathcal{E}\mathbb{1}) \cdot \mathbf{y}(x) = 0, \quad (12)$$

where $\mathbf{y}(x)$ is the vector formed by the radial functions $y_\ell(x)$, \mathbf{M} is the matrix representation of $\frac{1}{x^6} - \frac{\mathbf{L}^2}{x^2} + \mathcal{I} \frac{\cos^2 \theta - 1/3}{x^3}$ in the basis of the spherical harmonics, and $\mathbb{1}$ is the identity. In the present problem, the n considered channels correspond to the same dissociation limit E_0 lowered by the nonresonant field. For $\mathcal{E} < 0$, the energy levels are quantized and nondegenerate. The continuous spectrum is n -times degenerate and at each energy $\mathcal{E} \geq 0$, n linearly independent solutions are to be determined. We denote the physical wave functions, which are a solution of (12) and satisfy the boundary conditions, by a radial vector $\mathbf{z}(x)$, in contrast to $\mathbf{y}(x)$, which is a general solution of (12). The wave functions are calculated here by inward integration of the asymptotic Schrödinger equation, starting at a large separation x_{\max} with boundary conditions that depend on the energy \mathcal{E} . In the nodal line technique [22] one replaces the interaction at very small interatomic separations

by boundary conditions at the frontier between the inner and the asymptotic domains.

In detail, the physical radial wave function, i.e., all partial wave components $z_\ell(x)$, must vanish at the so-called nodal line [29,36] $x_0 \equiv x_0(\mathcal{E}, \ell, \mathcal{I})$, given by

$$x_0 = x_{00} + A\mathcal{E} + B\ell(\ell + 1) + C\mathcal{I}. \quad (13)$$

The parameters x_{00} , A , B , and C are characteristics of each atom pair. In particular, x_{00} is the position of a node of the field-free threshold s -wave function; it is determined unambiguously by the field-free s -wave scattering length in reduced units [19]. The parameter A accounts (to first order) for the energy dependence of the node position for wave functions with $\ell = 0$, whereas B describes the shift of the node of the threshold wave functions induced by the centrifugal term for different partial ℓ waves. The last term in x_0 accounts for the effects of the nonresonant field in the inner domain $x < x_{00}$ to first order in the field intensity. For more details on these parameters and how to choose them, the reader is referred to Ref. [22].

The wave functions $\mathbf{z}(x)$ are determined in two steps. First, a set of linearly independent particular solutions labeled $\mathbf{y}^j(x)$ satisfying the asymptotic boundary conditions in the n channels is obtained by inward integration. The number of such solutions is equal to n in the bound spectrum $\mathcal{E} < 0$ and to $2n$ in the continuous spectrum $\mathcal{E} \geq 0$. Second, the physical wave functions $\mathbf{z}(x)$ are constructed as linear combinations of the particular solutions $\mathbf{y}^j(x)$ such that they fulfill the boundary conditions at short range, on the nodal line.

For $\mathcal{E} < 0$, to obtain the energy of a bound state at a certain laser intensity \mathcal{I} , each of the n particular solutions $\mathbf{y}^j(x)$ is related to a specific channel ℓ in which the asymptotic boundary condition imposes an exponential decay, while in all other channels the radial functions vanish asymptotically. Imposing the boundary conditions at short range is equivalent to making a function vanish that depends on energy and that is defined in terms of the radial components $y_\ell^j(x_0)$ on the nodal lines. The roots, i.e., the energies for which the function vanishes, determine the bound levels, providing the quantization of the bound spectrum (see the Appendix in Ref. [22]). Analogously, to find at which intensity there is a bound state at a given energy, e.g., just below threshold, the zeros of a function of intensity have to be computed.

For $\mathcal{E} > 0$, there exists an infinite number of sets of physical solutions $\mathbf{z}^j(x)$ that can be calculated. For any specific problem, there is a most suitable choice for the n linear combinations of the $2n$ particular solutions that is defined by their asymptotic behavior. If the initial conditions of the inward integration are chosen properly, the relevant physical property can be determined in a straightforward way. To study the resonance structure of the continuum [22], the asymptotic behavior in each channel is described by combinations of regular and irregular spherical Bessel functions [37]. For that problem we impose that the $2n$ particular solutions be either regular or irregular spherical Bessel functions at x_{\max} in one channel and zero in all others. Among all possible sets of n physical combinations, we choose the standard form, in which the combination for a given channel asymptotically contains a regular component in this channel only and irregular

components in all channels. The n physical solutions $\mathbf{z}^j(x)$ are such linear combinations that vanish at the ℓ -dependent node position x_0 (13): These conditions allow for a direct determination of the reaction, scattering, and time delay matrices $\mathbf{K}(\mathcal{E})$, $\mathbf{S}(\mathcal{E})$, and $\mathbf{Q}(\mathcal{E})$, respectively, as described in Ref. [22]. The $\mathbf{Q}(\mathcal{E})$ matrix is well adapted to analyze shape resonances, by studying the energy dependence of its lowest eigenvalue [22]. In Sec. III B we show which particular solutions $\mathbf{y}(x)$ and which combinations $\mathbf{z}(x)$ are suitable for determining the scattering length, whereas in the Appendix we study how the outer boundary conditions affect the convergence of the calculation of the field-dressed scattering length.

B. Threshold wave functions and field-dressed scattering length

In order to determine the field-dressed scattering length $\tilde{a}(\mathcal{I})$, we construct a wave function at threshold ($\mathcal{E} = 0$) that varies linearly with x in the $\ell = 0$ channel and vanishes asymptotically in all other channels. We determine this wave function, as described above, by first constructing $2n$ particular solutions, denoted here by $\mathbf{f}_-^j(x)$ and $\mathbf{f}_+^j(x)$ with $1 \leq j \leq n$. The asymptotic behavior of the nonzero component of $\mathbf{f}_+^j(x)$ is divergent, $f_{+, \ell_j}^j(x) \sim x^{\ell_j+1}$, whereas $f_{-, \ell_j}^j(x)$ does not diverge, $f_{-, \ell_j}^j(x) \sim x^{-\ell_j}$. Several choices for the asymptotic form of $f_{\pm, \ell_j}^j(x)$ are possible. Here we will use pairs of analytical linearly independent threshold solutions of potentials $v_p^\ell(x) = \ell(\ell + 1)/x^2 - c_p/x^p$, chosen as approximations of the asymptotic *diagonal* term of the matrix $-\mathbf{M}$ in the channel ℓ_j in (12) (this choice is discussed in the Appendix, Sec. 1; see in particular Table III). The form of the physical wave functions $\mathbf{z}^j(x)$ is given by a linear combinations of a single asymptotically divergent solution and all n nondivergent solutions:

$$\mathbf{z}^j(x) = \sum_{j'=1}^n [\delta_{j',j} \mathbf{f}_+^{j'}(x) - \bar{\mathbf{M}}_{j',j}^j(x_0, x_{\max}) \mathbf{f}_-^{j'}(x)]. \quad (14)$$

The matrix $\bar{\mathbf{M}}$ (not to be confused with \mathbf{M}) is determined by the boundary conditions on the nodal lines and depends both on nodal lines and on x_{\max} . For a given atom pair, the nodal lines are fixed; in the following, we omit the x_0 dependence. One has $\bar{\mathbf{M}}(x_{\max}) = \mathbf{N}_-(x_{\max}) \cdot [\mathbf{N}_+(x_{\max})]^{-1}$, where, as in Ref. [22], the matrices $\mathbf{N}_+(x_{\max})$ and $\mathbf{N}_-(x_{\max})$ are defined by their matrix elements $[\mathbf{N}_\pm]_{\ell}^j(x_{\max}) = f_{\pm, \ell}^j(x_0)$, which are the values of all radial particular solutions on the nodal lines. The scattering length is obtained from the s -wave component of the physical solution $\mathbf{z}^{j=1}(x)$, which in our notation corresponds to $\ell_j = 0$ and is of the form

$$z_{\ell=0}^{j=1}(x) = f_{+, \ell=0}^{j=1}(x) - \sum_{j'=1}^n \bar{\mathbf{M}}_{j',1}^{j=1}(x_{\max}) f_{-, \ell=0}^{j'}(x). \quad (15)$$

In Eq. (15), the first term behaves asymptotically as $f_{+, \ell=0}^{j=1}(x) \rightarrow x$. The contributions to the sum of the radial components with $j' \geq 2$ vanish asymptotically at least as $1/x^2$, whereas for $j' = 1$, $f_{-, \ell=0}^{j=1}(x) \rightarrow 1$. Using the definition

$\mathcal{M}(x_{\max}) \equiv \overline{\mathbf{M}}_{j'=1}^{j=1}(x_{\max})$, one has, for sufficiently large x_{\max} ,

$$z_{\ell=0}^{j=1}(x_{\max}) \approx x_{\max} - \mathcal{M}(x_{\max}), \quad (16)$$

with

$$\lim_{x_{\max} \rightarrow \infty} \mathcal{M}(x_{\max}) = \tilde{a}(\mathcal{I}). \quad (17)$$

The field-dressed scattering length is unambiguously defined by (17), if the limit $x_{\max} \rightarrow \infty$ exists for $\mathcal{M}(x_{\max})$ and if it is independent of the boundary conditions of $f_{+, \ell}(x)$ and $f_{-, \ell}(x)$ at x_{\max} .

The nonresonant field introduces a coupling between different partial waves that vanishes asymptotically as $1/x^3$, so the definition of the scattering length becomes questionable. Indeed, for an isotropic potential decreasing as $-1/x^p$, the limit of $\tan \delta_{\ell}(k)/k^{2\ell+1}$ for $k \rightarrow 0$ does not exist for $2\ell + 3 \geq p$, with $\delta_{\ell}(k)$ being the asymptotic elastic scattering phase shift at the wave number k of the partial wave ℓ [27,38]. A $\log k$ term appears in its expression and a $\log x$ contribution in the threshold wave function. However, in the s -wave channel, there is no diagonal contribution of the nonresonant-field-induced interaction and the diagonal potential of (5) and (7) behaves asymptotically as $-1/x^6$. As emphasized in Refs. [24,28], the asymptotic behavior of a dipole-dipole interaction, equivalent to the field-induced term considered here, can be termed quasi-long-range, since it corresponds to an effective potential proportional to $-1/x^4$ for $\ell = 0$ and truly long-range effective potentials proportional to $-1/x^3$ for all other partial waves. The effective s -wave potential becomes more attractive as the laser intensity \mathcal{I} increases and never exhibits a centrifugal barrier. As a consequence, in spite of the $1/x^3$ dependence of the nonresonant field interaction, the definition of the field-dressed s -wave scattering length does not pose any formal difficulty.

We analyze the validity of the outlined procedure to compute the field-dressed scattering in detail in the Appendix. In particular, in the Appendix, Sec. 2, we provide an extension of the single-channel analytical two-potential approach originally developed by Levy and Keller [31,39] to determine the near-threshold elastic scattering phase shift in a long-range potential. For a potential $V(x)$ written as a sum of $1/x^p$ terms, we show that the expansion of $\mathcal{M}(x)$ in powers of $1/x$ contains a first term \mathcal{M}_0 , accounting for the short-range interaction, and a $1/x$ term, depending only on $V(x)$ and on its separation in two terms in the two-potential approach. This expansion allows for straightforward determination of \mathcal{M}_0 , i.e., of the field-dressed scattering length. We have compared the results of the single-channel Levy-Keller approach to systematic multichannel numerical calculations, with a small number of channels, various values of x_{00} and x_{\max} , and different asymptotic boundary conditions for $f_{\pm, \ell}(x)$. The comparison between analytical and numerical results reveals that there exists an optimal pair of functions for the initialization of the inward integration in the $\ell = 0$ channel, corresponding to a particularly rapid convergence of $\mathcal{M}(x_{\max})$. This allows for the computation of the field-dressed scattering length using a properly chosen x_{\max} (see the Appendix, Sec. 4).

IV. RESULTS

The interaction of an atom pair with nonresonant light modifies the effective potential of the vibrational motion such that a scattering state may become bound [14,15]. A bound state localized just at the dissociation limit for a particular nonresonant field intensity corresponds to a divergence of the scattering length as a function of the intensity. As a result, a nonresonant field can be used to control of the scattering length of a pair of colliding atoms.

To illustrate this control, we consider the two isotopes of strontium, ^{88}Sr and ^{86}Sr , with the largest natural abundance, 68% and 16%, respectively, and no nuclear spin. The scaling factors (4) adapted to the van der Waals interaction for the ^{88}Sr - ^{88}Sr and ^{86}Sr - ^{88}Sr atom pairs are reported in Table I of Ref. [22]. We have chosen these atom pairs due to their very different field-free s -wave scattering lengths, which also correspond to a different structure for shape resonances [21]. ^{88}Sr has an intraspecies scattering length close to zero, $\tilde{a}(\mathcal{I} = 0) = -2 a_0 = -0.013$ ru, and field-free shape resonances with $\ell = 4, 8, 12, \dots$, whereas the interspecies scattering length of ^{86}Sr - ^{88}Sr is very large, $\tilde{a}(\mathcal{I} = 0) = 100 a_0 = 0.664$ ru, and field-free shape resonances occur for $\ell = 2, 6, 10, \dots$ [20]. For ^{88}Sr - ^{88}Sr we derived realistic intensity-dependent nodal lines from the wave functions calculated in a single-channel diagonalization of the full Hamiltonian [Eq. (1)] introduced in Ref. [14]. For ^{86}Sr - ^{88}Sr , for which there are no previous reliable theoretical or experimental data, we used universal analytical parameters depending only on the s -wave scattering length [22].

In the following we use the asymptotic boundary conditions BC24*, defined in the Appendix, Sec. 1, as initial conditions for the inward integration of the asymptotic Schrödinger equation.

A. Scattering of ^{88}Sr atoms: Realistic nodal lines

We have performed calculations with 11 channels, using different x_{\max} in different channels. We have chosen x_{\max} such that we obtain, at this point and for the largest intensity considered, $\mathcal{I} = 40$ ru (25 GW cm $^{-2}$), an ℓ purity close to one for each adiabatic eigenvalue. Here x_{\max} ranges from $x_{\max} = 20.9$ ru (3160 a_0) for $\ell = 0$ to $x_{\max} = 1.7$ ru (255 a_0) for $\ell = 20$. The largest systematic error of the scattering length is obtained from the \mathcal{I}^2/x_{\max} coefficient of the expansion of $\mathcal{M}(x_{\max})$ given in Table V of the Appendix. For $\mathcal{I} = 40$ ru and $x_{\max} = 20.9$ ru used for $\ell = 0$, this error is of the order of -0.04 ru, which is absolutely negligible on the scale of the figures presented below.

The field-dressed scattering length of ^{88}Sr atoms is shown in Fig. 1 together with the position of shape resonances and bound states of $^{88}\text{Sr}_2$ as a function of the nonresonant light intensity (top panel of Fig. 1). The almost linear character of the energy dependence of the shape resonance positions is discussed in Ref. [23]. All crossings between resonances or bound states are in fact anticrossings. We introduce diabaticized labels $\tilde{\ell}$, where ℓ is the orbital momentum of the field-free states. The field-dressed scattering length exhibits divergences or poles at the nonresonant light intensities for which a bound state is located exactly at the dissociation threshold. This is indicated by the dashed arrows in Fig. 1. To determine the

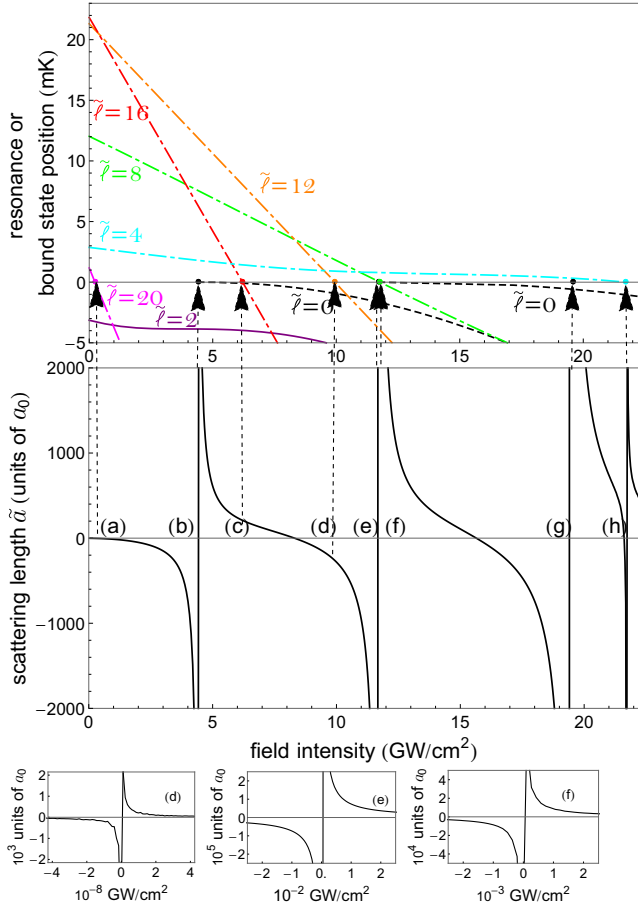


FIG. 1. Comparison of the intensity dependence of bound-state energies and shape resonance positions (top) to the field-dressed scattering length of ^{88}Sr atoms (middle and bottom). The resonances and bound states are characterized by diabatized labels $\tilde{\ell}$ (see the text). Broad poles (b), (e), and (g) correspond to regular scattering states with $\tilde{\ell} = 0$ becoming bound. Narrow features (a), (c), (d), (f), and (h) are field-shifted shape resonances with $\tilde{\ell} = 20, 16, 12, 8,$ and 4 , respectively. Poles (d)–(f), which do not clearly appear in the upper part, are shown in the bottom diagrams, with subtraction of the background value of scattering length $a_1 + a_2\mathcal{I}$ and of the resonance intensity $\mathcal{I}_{\text{pole}}$ [see (18)]. Poles (a) and (c) are too narrow to obtain a precise shape.

width w of the poles, the field-dressed scattering length is fitted to the expression

$$f(\mathcal{I}) = a_1 + a_2\mathcal{I} + \frac{w}{(\mathcal{I} - \mathcal{I}_{\text{pole}})}, \quad (18)$$

where we have introduced an intensity-dependent background scattering length $a_1 + a_2\mathcal{I}$ and $\mathcal{I}_{\text{pole}}$ is the nonresonant light intensity at which the divergence occurs. The positions and widths of the singularities of the scattering length are summarized in Table I.

The new bound states can be classified according to their rotational quantum number. Type (i) has $\tilde{\ell} > 0$ and corresponds to a shape resonance with vanishing width that is pushed below threshold as the nonresonant field intensity increases. The slope of the bound-state energy as a function of the nonresonant field intensity is very large and correspondingly the pole of the

TABLE I. For the pair ^{88}Sr - ^{88}Sr in nonresonant light, features of the poles of the field-dressed scattering length (see Fig. 1): diabatized label $\tilde{\ell}$ and position and width in reduced units (\mathcal{I} and w) and in physical units (I and W). A pole denoted by (S) is a shape resonance $\tilde{\ell} > 0$ becoming a bound state as the intensity increases. A pole with $\tilde{\ell} = 0$ is a supplementary state, which appears because the adiabatic s -wave potential becomes deeper. The calculations are done for $n = 11$ coupled channels with $\ell_{\text{max}} = 20$. Realistic nodal lines (see the text) are used.

Pole	$\tilde{\ell}$ label	$\mathcal{I}_{\text{pole}}$ (ru)	I_{pole} (GW cm^{-2})	w (ru)	W (GW cm^{-2})
(a)	20 (S)	0.368	0.234	too small	too small
(b)	0	6.93	4.41	3.43	2.18
(c)	16 (S)	9.77	6.21	$\sim 10^{-12}$	$\sim 10^{-12}$
(d)	12 (S)	15.7	9.96	2.21×10^{-8}	1.41×10^{-8}
(e)	0	18.4	11.7	7.62	4.89
(f)	8 (S)	18.5	11.8	0.0916	0.0583
(g)	0	30.5	19.4	13.6	8.65
(h)	4 (S)	34.2	21.7	0.641	0.408

scattering length has very small width. Type (ii) is a regular scattering state with $\tilde{\ell} = 0$ that becomes bound. This is due to the deepening of the field-dressed adiabatic s -wave potential, which can accommodate an additional bound state. For a supplementary bound state with $\tilde{\ell} = 0$, the width of the pole is very broad, because the energy of such a state remains very close to the dissociation limit in a large range of intensities; see the dependence of the bound-state energy as a function of intensity in Fig. 1 that starts tangentially to the threshold.

The pole structure of the field-dressed scattering length in Fig. 1 appears to be very similar to that observed for magnetic Feshbach resonances [5]. However, there are two essential differences. First, in a magnetic Feshbach resonance, there are at least one open and one closed channel with different dissociation limits, whereas in the present problem, all channels have the same dissociation limit. Magnetic Feshbach resonances arise from the coupling between a bound state in the closed channel and degenerate scattering states in the open one. In contrast, the divergence of the scattering length as a function of the nonresonant field appears when a shape resonance becomes bound. Second, for magnetic Feshbach resonances, there is no equivalent to regular scattering states being accommodated as bound states in a modified s -wave potential.

The resonance structure in the energy dependence of the near-threshold cross section has been previously analyzed in Refs. [25,40]. In particular, for bosons, the resonances of the $\ell = 0, m = 0$ lowest adiabatic potential, which extend over a broad range of the cutoff radii modeling the short-range interaction, correspond to our type (i) poles. They produce an enhancement of the partial cross section averaged over the polarization direction by about two orders of magnitude.

B. Interspecies scattering of ^{86}Sr and ^{88}Sr atoms: Universal nodal lines

The power of the asymptotic model lies in the possibility to predict, at least roughly, the intensity dependence of the field-dressed scattering length for any atom pair. The field-free

s -wave scattering length enters as the only free parameter; it determines the universal nodal lines [21]. A universal nodal line refers to Eq. (13) with the three parameters A , B , and C taking universal values. In particular, analytical formulas for the coefficients A and B in Eq. (13) are deduced from the universal model of Ref. [16], which consists in a $-1/x^6$ potential limited by an infinite repulsive wall at a distance $x_{0G} \rightarrow 0$. The shift of the node located at x_{00} , which is due to the contribution of the kinetic $A\mathcal{E}$ and centrifugal $B\ell(\ell+1)$ energies in the range $x_{0G} \leq x \leq x_{00}$, can be evaluated using the WKB approximation [41]. Specifically, the scattering length fixes the parameter x_{00} in (13) and is used to estimate the universal coefficients $A^G = -(x_{00})^7/8$ and $B^G = (x_{00})^5/4$ [21]. For nodes at not too short range, the obtained values for A^G and B^G are comparable to those obtained from fitting to experimental data [29,30]. There is also an analytical formula for the parameter C^G accounting for the contribution of the nonresonant field at short range [22].

We now use the asymptotic model with these universal nodal lines to predict the intensity dependence of the field-dressed interspecies scattering length of ^{86}Sr - ^{88}Sr . The calculations were performed with $n = 5$ coupled channels, i.e., $\ell_{\max} = 8$.

For all channels, we have used $x_{\max} = 40$ ru ($6000a_0$). The results are presented in Fig. 2 and the positions and widths of the poles are summarized in Table II.

As for the intraspecies scattering of ^{88}Sr atoms, there is a strong difference in the widths of the two types (i) and (ii) of poles in Fig. 2. The avoided crossings among bound states are very broad and widely avoided. Due to one of these anticrossings, the $\tilde{\ell} = 6$ resonance crosses the threshold twice. As a consequence, we obtain a negative width for the second pole with $\tilde{\ell} = 6$ in the scattering length (see Table II). Note that the scattering length is large and positive when there is a bound level close to threshold, which in this case occurs for $\mathcal{I} < \mathcal{I}_{\text{pole}}$.

C. Prediction of the field-dressed scattering length for any pair of atoms

The asymptotic model with universal nodal lines can be used to predict the intensity-dependence of the scattering length for any pair of atoms, based on either the field-free scattering length or the node position of the field-free s -wave threshold wave function. This is illustrated in Fig. 3, where, in the top panel, x_{00} corresponds to the sixth node (counted from the outside) of the s -wave threshold wave function. The results have been calculated using $n = 5$ channels, i.e., $\ell_{\max} = 8$. We can read off from Fig. 3 the nonresonant light intensities at which a new bound level appears at the dissociation limit and, equivalently, a pole occurs in the field-dressed scattering length $\tilde{a}(\mathcal{I})$: Any atom pair is characterized by a value of either x_{00} or $\tilde{a}(\mathcal{I} = 0)$. Drawing a horizontal line at this value, a pole in the field-dressed scattering length occurs when one of the black curves crosses the horizontal line. We have included the horizontal lines corresponding to infinite field-free scattering length as well as those for ^{88}Sr - ^{88}Sr and ^{86}Sr - ^{88}Sr in Fig. 3 for illustration.

For x_{00} , in the top panel of Fig. 3, we encounter two types of states at the dissociation threshold. For shape resonances

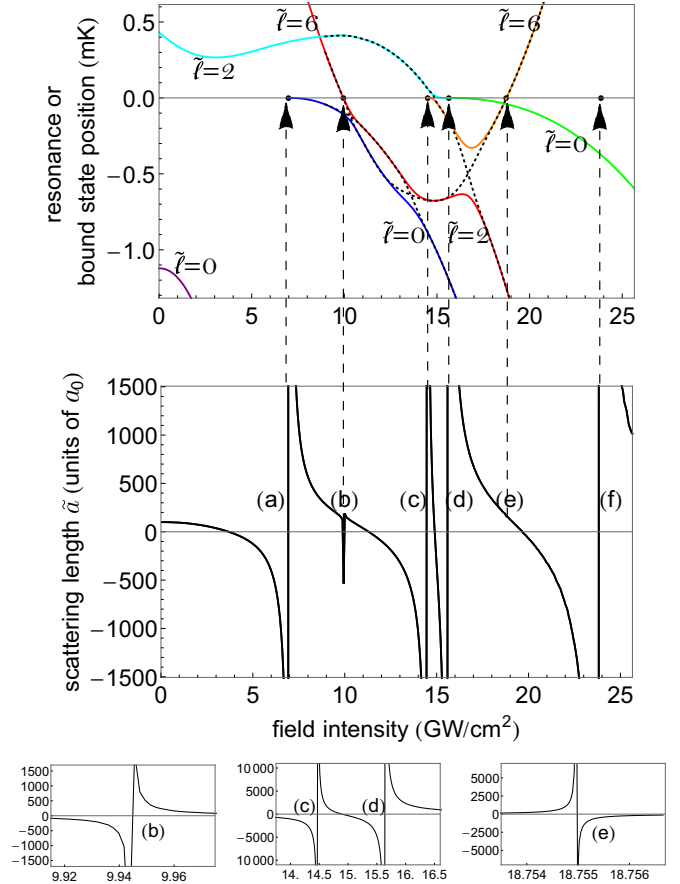


FIG. 2. Comparison of the intensity dependence of bound-state energies and shape resonance positions (top) to the field-dressed interspecies scattering length of ^{86}Sr and ^{88}Sr atoms (middle and bottom). Due to the wide avoided crossings, it is impossible to match colors and labels; diabaticized curves are indicated by black dotted lines. The broad poles of the scattering length (a), (d), and (f) correspond to regular scattering states with $\tilde{\ell} = 0$ becoming bound, whereas narrow ones (b), (c), and (e) are shape resonances with $\tilde{\ell} = 6, 2$, and 6 , respectively, crossing the dissociation limit, as in Fig. 1. The narrowest poles are shown in the bottom diagrams with subtraction of the background scattering length for poles (b) and (e). In this part, axis labels are omitted, since they are identical to those of the diagram just above.

TABLE II. Same as Table I but for the pair ^{86}Sr - ^{88}Sr . The calculations correspond to an $n = 5$ coupled-channel model (with $\ell_{\max} = 8$). Universal nodal lines (see the text) are used. The exceptional shape of the resonance (e) in Fig. 2 explains the sign of its width (see the text).

Pole	$\tilde{\ell}$ label	$\mathcal{I}_{\text{pole}}$ (ru)	I_{pole} (GW cm^{-2})	w (ru)	W (GW cm^{-2})
(a)	0	10.9	6.99	5.29	3.39
(b)	6 (S)	15.5	9.94	0.0270	0.0173
(c)	2 (S)	22.6	14.5	3.74	2.40
(d)	0	24.4	15.6	7.51	4.81
(e)	6 (S)	29.2	18.8	-0.00230	-0.00148
(f)	0	37.2	23.8	18.9	12.1

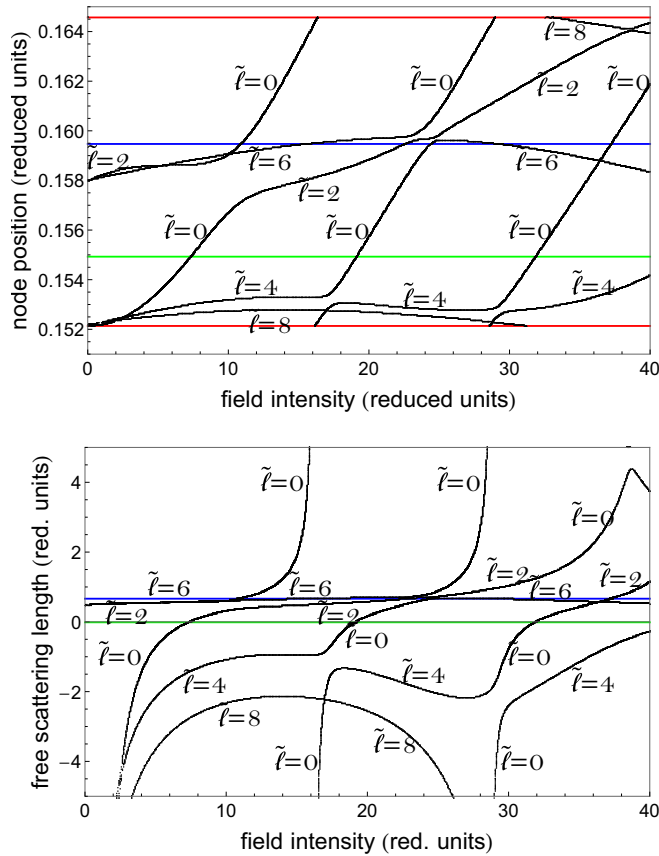


FIG. 3. Nonresonant light intensity, in reduced units, leading to a divergence of the field-dressed scattering length. Each atom pair is characterized either by a node position x_{00} of its field-free s -wave threshold wave function (top panel) or by its field-free scattering length (bottom panel), indicated by horizontal lines in either diagram. The red lines corresponds to an infinite field-free reduced scattering length, whereas the green and blue lines represent ^{88}Sr - ^{88}Sr and ^{86}Sr - ^{88}Sr , respectively. A diabatic labeling is used. Here $\tilde{\ell} > 0$ describes a shape resonance becoming bound at the dissociation threshold and $\tilde{\ell} = 0$ denotes a regular scattering state that turns into a supplementary bound level in the adiabatic field-dressed s -wave potential.

($\tilde{\ell} > 0$) pushed below threshold [type (i) pole], atom pairs with similar values of x_{00} have very different pole positions and the slope of x_{00} as a function of the nonresonant field intensity is very small. This shows that the position, or energy, of a field-dressed shape resonance strongly depends on the short-range interaction. An exception is observed for the $\tilde{\ell} = 2$ states at $\mathcal{I} > 10$ ru and the $\tilde{\ell} = 4$ states at $\mathcal{I} > 30$ ru, because the direct coupling between the $\ell = 2$ and $\ell = 0$ ($\ell = 2, 4$, and 6) channels is very large. In contrast, for regular scattering states becoming bound in the modified s -wave potential [type (ii) poles], the field intensity characterizing the pole positions varies rapidly and almost linearly with x_{00} . As a result, the appearance of such a bound state depends mainly on the long-range properties of the field-dressed adiabatic s -wave potential and only to a lesser extent on the field-free scattering length. This can be seen in the bottom graph of Fig. 3, where the $\tilde{\ell} = 0$ poles appear as almost vertical curves.

According to the field-free analytical model of Ref. [42], bound states with $\ell = 4p$, where $p \geq 0$ and an integer, are located at threshold for an infinite scattering length, whereas for scattering lengths of $\tilde{a}(\mathcal{I} = 0) = 0.48$ ru and $x_{00} = 0.158$ ru bound levels with $\ell = 2 + 4p$ are located at the dissociation limit. These predictions are approximately reproduced in our asymptotic model with universal nodal lines in the field-free case (cf. Fig. 3).

The node position of $x_{00} = 0.1595$ ru is associated with interspecies scattering of ^{86}Sr and ^{88}Sr atoms (blue vertical line in the top panel of Fig. 3) and Fig. 3 confirms the results of Table II, which were also calculated with universal nodal lines. A field-free scattering length of -0.013 ru and $x_{00} = 0.1549$ ru describe intraspecies scattering of ^{88}Sr atoms (green horizontal line). The asymptotic model with universal nodal lines predicts three regular s -wave scattering states becoming bound at $\mathcal{I} \approx 7, 16$, and 32 ru, i.e., very close to the nonresonant field intensities obtained with realistic nodal lines for which the parameters were adjusted to reproduce the field-free scattering length (see Table I). This confirms the slight dependence of the corresponding poles of the field-dressed scattering length on the nodal lines. In contrast, for $\tilde{\ell} = 4$ and $\tilde{\ell} = 8$, the states obtained with universal nodal lines are never located at the dissociation limit, unlike the results obtained with realistic nodal lines in Table I. As discussed above, the energies of field-free shape resonances strongly depend on the node position in the ℓ channel, i.e., on the B coefficient in (13), a sensitivity that increases for higher partial waves due to the factor $\ell(\ell + 1)$. Our present findings are in line with Ref. [22], where an overestimation of the field-free shape resonance positions with universal nodal lines was observed.

The actual nonresonant field intensities that are required to control the scattering length in strontium are rather large: 4.4 and 7.0 GW cm^{-2} for intraspecies and interspecies scattering, respectively. Control with a significantly smaller nonresonant field intensity may be expected for atom pairs with a field-free scattering length between 0.48 ru and that of ^{86}Sr and ^{88}Sr atoms, 0.664 ru (or, correspondingly, x_{00} between 0.158 and 0.1595 ru): Since $\tilde{a}(\mathcal{I} = 0) = 0.48$ ru is the value for which shape resonances $\tilde{\ell} = 2, 6, \dots$ are located at threshold, a comparatively small nonresonant field intensity is sufficient to cross the $\tilde{\ell} = 2, 6$ curves in Fig. 3 by the horizontal line for an atom pair with a slightly larger field-free scattering length. According to [21], field-free scattering lengths within this range are found for the intraspecies scattering of ^7Li in the ground singlet electronic state and of ^{41}K and ^{87}Rb in either the ground singlet or lowest triplet state. Interspecies scattering of ^6Li - ^{40}K , ^6Li - ^{41}K , ^7Li - ^{87}Rb , and ^7Li - ^{133}Cs in the ground singlet electronic state and ^6Li - ^7Li and ^{23}Na - ^{87}Rb in the lowest triplet state also exhibits field-free scattering lengths within this range. The prospect of smaller nonresonant field intensities required than for the control of interspecies scattering in strontium comes, however, with the consequence that the pole of the scattering length will be narrow since a shape resonance, and not a regular scattering state (with $\tilde{\ell} = 0$), is pushed below the dissociation threshold.

In contrast, for atom pairs with negative field-free scattering length, the nonresonant field intensity must be at least larger than 2 ru. The corresponding large intensities make the control of the scattering length with a nonresonant field

more challenging for these atom pairs. For the example of intraspecies scattering of ^{85}Rb in the lowest triplet state, one would expect an $\tilde{\ell} = 0$ divergence at $\mathcal{I} = 3$ ru (0.78 GW cm^{-2}) and an $\tilde{\ell} = 4$ divergence at $\mathcal{I} = 5$ ru (1.3 GW cm^{-2}). The $\tilde{\ell} = 0$ pole will be broad and could be exploited for nonresonant light control of the scattering.

V. CONCLUSION

An asymptotic model has been used to analyze the scattering of two ultracold atoms in a nonresonant laser field. It provides a realistic approximation to the field-dressed scattering length. The pair of atoms interacts with the nonresonant light via its polarizability anisotropy such that the potential acquires an anisotropic $1/R^3$ asymptotic behavior. The asymptotic Hamiltonian is formally equivalent to the one describing the anisotropic dipole-dipole scattering in ultracold gases of atoms or molecules. While for a potential with an isotropic $1/R^3$ long-range dependence the scattering length cannot be defined, the anisotropy induced by nonresonant light does not introduce a direct $1/R^3$ interaction term in the s -wave channel. In second-order perturbation theory the effective s -wave potential decreases as $1/R^4$ and the scattering length can be defined without any formal difficulty. The field-dressed scattering length is determined from a threshold wave function that shows a linear variation with R in the s -wave channel and does not diverge asymptotically for all higher partial waves.

In more detail, from the zero-energy scattering wave function, we have defined a quantity $\mathcal{M}(x)$ that tends to the scattering length for large x . We first determined $\mathcal{M}(x)$ analytically for a single-channel model and a potential given by a multipole expansion. We predict in this way the expansion of $\mathcal{M}(x)$ in powers of $1/x$ for various choices of reference functions, with different asymptotic behavior. In particular, a suitable choice of the reference functions allows us to cancel the $1/x$ term. Then, for various atom pairs (i.e., various x_{00} or various field-free scattering length), we calculated $\mathcal{M}(x)$ numerically for a range of values of x_{max} . Fitting $\mathcal{M}(x_{\text{max}})$ has allowed us to deduce an expansion of $\mathcal{M}(x_{\text{max}})$ into a series of $1/x_{\text{max}}$. We have found the results of the numerical fits to agree well with the analytical results when considering an expansion of both the s -wave adiabatic potential and the nonadiabatic coupling terms in powers of $1/x$, the latter being clearly non-negligible. The analysis has allowed us to estimate the uncertainty of the calculated scattering length when it is obtained from a single inward integration with judicious asymptotic boundary conditions at a value of x_{max} that is not too large.

We have shown that the scattering properties of an atom pair can be controlled by tuning the nonresonant field intensity. The scattering length diverges each time a field-dressed bound state reaches the threshold. We have encountered two types of divergences, with very different properties. On the one hand, narrow divergences appear when a shape resonance with partial wave $\ell > 0$ becomes bound. The corresponding nonresonant field intensity strongly depends on the interaction of the atom pair in the inner domain. On the other hand, broad divergences appear when a deepening of the adiabatic field-dressed s -wave potential results in additional bound levels in the field-dressed s -wave channel. The corresponding

intensities vary approximately linearly with the node position x_{00} , which replaces the inner part of the potential. The periodicity of the intensities at which the successive additional levels appear is almost independent of the atom pair, since it is a characteristic of the long-range part of the field-induced interaction [25].

To illustrate the validity of the asymptotic method and the capability of nonresonant light to control the scattering length, we have considered the intraspecies scattering of ^{88}Sr atoms and the interspecies scattering of ^{86}Sr and ^{88}Sr atoms as prototype systems. They have, respectively, a small and large field-free scattering length and therefore very different scattering properties. In contrast to shape resonances, where the intensity dependence of the resonance position was found to be rather different for the two cases [22,23], the intensity dependence of the field-dressed scattering length turns out to be very similar, in particular for broad poles of the scattering length. This is explained by the fact that these poles occur when a regular scattering state becomes bound, which is dictated almost exclusively by the field-induced dipole-dipole term, independently of the short-range interaction. In addition to strontium, we have considered an arbitrary pair of atoms, characterized only by the field-free scattering length, and we have predicted, in a completely general way, at which field intensity the field-dressed scattering length exhibits a divergence. This allows us to estimate the nonresonant light intensity required to tune the scattering length for a given atom pair, provided the field-free scattering length is known.

In view of experimental realization of nonresonant light control, the high intensities that are required can be achieved by tightly focused YAG or CO_2 lasers. For strontium, they are both far detuned from any transition involving the electronic ground state, even though their frequencies are very different, 1064 nm compared to 10 μm . The coupling to the nonresonant light will therefore be dominated by the static polarizabilities and dynamic polarizability effects are negligible. There is no advantage of one of the two wavelength choices over the other in terms of heating due to photon scattering. With a heating rate of less than 1 $\mu\text{K/s}$ for $I = 10^9 \text{ W/cm}^2$, estimated in terms of the atomic photon scattering rates [43], heating is negligible for 1064 nm and even more so for longer wavelengths. Note that this picture changes when alkali-metal atoms are involved. Depending on the species, dynamic polarizability effects may become important for 1064-nm light, which might decrease the required intensity but increase heating rates. In this case, a full calculation for the specific atom pair will be required since it is not straightforward to derive an asymptotic model for the dynamic polarizability. One might also wonder whether multiphoton processes beyond the two-photon effects that we have accounted for in our model come into play. However, despite the high intensities, the overall light-matter coupling is still sufficiently small for low-order perturbation theory to be valid [23]. For example, multiphoton ionization of strontium would require seven photons of 1064 nm and many more for a CO_2 laser. Multiphoton processes can therefore be ruled out.

In future work, it will be important to consider the scattering of fermionic atoms. For a pair of polarized fermionic atoms colliding in odd-parity waves only, all channels involve an asymptotic $1/R^3$ potential and, at ultracold temperature, the usual p -wave scattering volume describing the collision

TABLE III. Analytical expression (column 2) of the pairs of linearly independent functions used either as asymptotic boundary conditions (BC, labeled in column 1) at x_{\max} in the channel ℓ or as a reference pair of $\ell = 0$ functions in the analytical model (φ and ψ being, respectively, the divergent and the nondivergent ones). The symbols α , ρ , and γ that appear in column 2 are given in columns 4, 5, and 6. These functions are analytical solutions at threshold ($\mathcal{E} = 0$) of the single- ℓ -channel Schrödinger equation with the potential $v_p^\ell(x) = \ell(\ell + 1)/x^2 - c_p/x^p$ [45], with p given in the third column. The functions behave asymptotically as $x^{\ell+1}[1 + O(c_p x^q)]$ and $x^{-\ell}[1 + O(c_p x^q)]$ for the divergent (upper sign or row 1) and nondivergent (lower sign or row 2) case, respectively, with q given in column 7. For free spherical waves, labeled by BC2 with $p = 0$ and $c_p = 0$, the functions are everywhere equal to their asymptotic limit.

Label	Function	p	α	ρ	γ	q
BC2	$x^{\ell+1}$	0				0
BC2	$x^{-\ell}$					
BC26	$\gamma \sqrt{x} J_{\mp\alpha}(\rho)$	6	$(2\ell + 1)/4$	$\sqrt{c_p}/(2x^2)$	$(\sqrt{c_p}/4)^{\pm\alpha} \Gamma(1 \mp \alpha)$	-4
BC24	$\gamma \sqrt{x} J_{\mp\alpha}(\rho)$	4	$(2\ell + 1)/2$	$\sqrt{c_p}/x$	$(\sqrt{c_p}/2)^{\pm\alpha} \Gamma(1 \mp \alpha)$	-2

cannot be defined. In another work [44], the theoretical tools developed here for s -wave scattering will be adapted to describe the near threshold p -wave scattering of two fermionic atoms in a nonresonant laser field.

ACKNOWLEDGMENTS

R.G.-F. gratefully acknowledges financial support through Project No. FIS2014-54497-P (MINECO) and the Grants No. FQM-207 and No. P11-FQM-7276 from Junta de Andalucía.

APPENDIX: COMPUTATION OF THE FIELD-DRESSED SCATTERING LENGTH

In this appendix we discuss in detail how to compute the field-dressed scattering length. The analytical functions chosen to initialize the inward integration, by boundary conditions (BCs) at x_{\max} , are specified in Sec. 1. In Sec. 2 we suggest an extension of the single-channel approach by Levy and Keller [31,39] to the threshold wave function in order to calculate analytically the asymptotic phase shift for near-threshold elastic scattering in a long-range potential written in a multipole expansion. Using this extension, we obtain analytical asymptotic expansions of $\mathcal{M}(x_{\max})$ in powers of $1/x_{\max}$ for different asymptotic boundary conditions. The adiabatic s -wave potential and the nonadiabatic contributions are examined in Sec. 3. For a small number of channels, we perform systematic calculations of $\mathcal{M}(x_{\max})$ and numerical fits to obtain the coefficients of the $\mathcal{M}(x_{\max})$ expansion in powers of $1/x_{\max}$, which are compared to the analytical results in Sec. 4.

1. Asymptotic boundary condition for the inward integration

The pairs of analytical functions defined in Table III provide the asymptotic boundary conditions at x_{\max} in the channel ℓ , i.e., initial conditions for inward integration in channel ℓ . They are solutions of the Schrödinger equation associated with the asymptotic potential $v_p^\ell(x) = \ell(\ell + 1)/x^2 - c_p/x^p$, with $p > 2$, for zero energy [27,45]. We present several choices,¹ generally expressed in terms of Bessel functions, which behave

¹In principle, any pair of functions with different logarithmic derivatives at x_{\max} could be used for each ℓ to obtain a set of solutions, but the asymptotic behavior of the solutions would in general be difficult to analyze.

asymptotically as $x^{\ell+1}[1 + O(c_p x^q)]$ and $x^{-\ell}[1 + O(c_p x^q)]$, respectively.

The labels are chosen as follows. The boundary conditions BC2 use $c_p = 0$ and $p = 0$ such that $v_p^\ell(x)$ reduces to the centrifugal term. The centrifugal term plus the van der Waals contribution, i.e., $p = 6$, is labeled by BC26. The case BC24 with $p = 4$ is well adapted to represent the effective field-dressed s -wave potential in a multichannel description, because both the adiabatic potential and the nonadiabatic couplings vanish asymptotically as $1/x^4$ (see Sec. 3).

2. Two-potential approach to analytically determine the asymptotic behavior of $\mathcal{M}(x_{\max})$

We extend the two-potential method suggested originally by Levy and Keller [31,46,47] to determine, in a single-channel approach, the asymptotic behavior of $\mathcal{M}(x_{\max})$ for the threshold s -wave solution of the Schrödinger equation involving an asymptotic potential $V(x) = -c_4/x^4 - c_5/x^5 - c_6/x^6$. Following this method, a second potential $V_f(x)$ is defined to determine a pair of reference functions $\varphi(x)$ and $\psi(x)$, which are linearly independent, analytical threshold solutions of this potential. According to Ref. [31], the s -wave solution at threshold of the Schrödinger equation with the potential $V(x)$ can be written as

$$u(x) = A(x)[\varphi(x) - \psi(x)\mathcal{M}(x)], \quad (\text{A1})$$

with the condition

$$\frac{du(x)}{dx} = A(x) \left[\frac{d\varphi(x)}{dx} - \frac{d\psi(x)}{dx} \mathcal{M}(x) \right]. \quad (\text{A2})$$

The Schrödinger equation for $u(x)$ with the condition (A2) is equivalent to

$$\frac{d\mathcal{M}(x)}{dx} = -\frac{V_p(x)}{W} [\varphi(x) - \psi(x)\mathcal{M}(x)]^2, \quad (\text{A3a})$$

$$\frac{1}{A(x)} \frac{dA(x)}{dx} = -\frac{V_p(x)\psi(x)}{W} [\varphi(x) - \psi(x)\mathcal{M}(x)], \quad (\text{A3b})$$

with $V_p(x) = V(x) - V_f(x)$ and W the Wronskian of $\varphi(x)$ and $\psi(x)$.

Here we choose $V_f(x) = 0$ or $V_f(x) = -c_p/x^p$ with $p \geq 4$ and we use for $\varphi(x)$ and $\psi(x)$ the pairs of analytical functions $\ell = 0$ defined in Sec. 1. Since for each p the asymptotic limits

TABLE IV. Analytical expansion in powers of $1/x$ of $\mathcal{M}(x)$ (column 4), which characterizes the s -wave threshold solution $u(x)$ [Eq. (A1)] of the single-channel Schrödinger equation in the potential $V(x) = V_f(x) + V_p(x) = -c_4/x^4 - c_5/x^5 - c_6/x^6$ when $u(x)$ is written in terms of two reference functions (labeled in column 1), which are threshold solutions of the potential $V_f(x)$ (column 2). $V_p(x)$ is given in column 3 and the expression of the reference functions is given in Table III.

Label	$V_f(x)$	$V_p(x)$	$\mathcal{M}(x)$
BC2	0	$-c_4/x^4 - c_5/x^5 - c_6/x^6$	$\mathcal{M}_0 + c_4/x + (c_5 + c_4\mathcal{M}_0)/x^2 + O(1/x^3)$
BC26	$-1/x^6$	$-c_4/x^4 - c_5/x^5 - (c_6 - 1)/x^6$	$\mathcal{M}_0 + c_4/x + (c_5 + c_4\mathcal{M}_0)/x^2 + O(1/x^3)$
BC24	$-c_{4f}/x^4$	$-(c_4 - c_{4f})/x^4 - c_5/x^5 - c_6/x^6$	$\mathcal{M}_0 + (c_4 - c_{4f})/x + [c_5 + (c_4 - c_{4f})\mathcal{M}_0]/x^2 + O(1/x^3)$

of the reference functions are pure centrifugal wave functions, the scattering length \tilde{a} is the limit of $\mathcal{M}(x)$ for $x \rightarrow \infty$ [see Eq. (17)]. For a chosen pair of reference functions $[\varphi(x)$ and $\psi(x)]$ associated with a given potential $V_f(x)$, the asymptotic form of $\mathcal{M}(x)$ is expanded in powers of $1/x$. The coefficients of this expansion are obtained analytically by identifying the terms with the same power of $1/x$ in Eq. (A3a). It is obvious that this asymptotic analysis does not determine the constant coefficient \mathcal{M}_0 , which does not appear on the left-hand side of the equation. This is not surprising since this coefficient depends on the short-range part of $V(x)$. Conversely, the other terms depend only on the potentials $V_p(x)$ and $V_f(x)$. The analytical expansion of $\mathcal{M}(x)$, corresponding to the labels of Table III, is reported in Table IV. To $O(1/x^3)$, $\mathcal{M}(x)$ does not depend on the coefficient of the van der Waals interaction $-c_6/x^6$. The coefficient of $1/x$ depends only on the $1/x^4$ terms in $V_p(x)$ and $V_f(x)$. The convergence of the $\mathcal{M}(x)$ expansion can be then controlled by a proper choice of $V_f(x)$. For example, the case BC24 allows us to cancel the $1/x$ term in the expansion of $\mathcal{M}(x)$ by imposing $c_{4f} = c_4$, i.e., by using reference functions related to the total $-c_4/x^4$ contribution to $V(x)$.

As mentioned above, this asymptotic analysis does not determine the constant coefficient of the expansion \mathcal{M}_0 , i.e., the scattering length \tilde{a} . However, if one introduces the analytical expansion of $\mathcal{M}(x)$ in powers of $1/x$ into Eq. (A3b), one can obtain the analytical expansion of $A(x)$ in powers of $1/x$ (including the \mathcal{M}_0 term) and then of the wave function $u(x)$ itself, which obviously does not depend on the choice of reference functions. One can finally compare the values of \mathcal{M}_0 corresponding to different reference pairs: It appears that the value of \mathcal{M}_0 does not depend on the choice of the reference pair.

3. Adiabatic s -wave potential and nonadiabatic effects

In Table IV one can see that, when using the reference pair BC24 and $c_{4f} = c_4$, $\mathcal{M}(x)$ converges as $1/x^2$ instead of $1/x$ in the other cases. One may expect an increased convergence of the numerical multichannel calculations when using the BC24 condition in the s channel. To determine the optimal c_4 value, we calculate the expansion in powers of $1/x$ of the effective s -wave potential in the matrix $-\mathbf{M}(x)$ in (12) and of the nonadiabatic contributions to this potential in an n -channel description.

For two coupled channels, with $\ell = 0$ and 2, an analytical expression can be found for the field-dressed adiabatic s -wave potential $v_{\text{ad}}^{\ell=0}(x)$ of the Hamiltonian (5). It is obtained as the lowest eigenvalue of the 2×2 matrix $-\mathbf{M}(x)$ appearing in (12)

and given by the van der Waals interaction plus a series of the form \mathcal{I}^{q-2}/x^q ,

$$v_{\text{ad}}^{\ell=0}(x) = -\frac{1}{x^6} - \frac{2}{135} \frac{\mathcal{I}^2}{x^4} - \frac{4}{8505} \frac{\mathcal{I}^3}{x^5} + \frac{58}{2679075} \frac{\mathcal{I}^4}{x^6} + O\left(\frac{\mathcal{I}^5}{x^7}\right). \quad (\text{A4})$$

The diagonal contribution of the nonadiabatic coupling, due to the x dependence of the corresponding adiabatic eigenvector $\Phi(x)$, i.e., the kinetic energy mean value $\langle \Phi | d^2 \Phi / dx^2 \rangle$, reads

$$v_{n-\text{ad}}(x) = -\frac{1}{405} \frac{\mathcal{I}^2}{x^4} - \frac{8}{25\,515} \frac{\mathcal{I}^3}{x^5} + \frac{64}{2\,679\,075} \frac{\mathcal{I}^4}{x^6} + O\left(\frac{\mathcal{I}^5}{x^7}\right). \quad (\text{A5})$$

Note the importance of this nonadiabatic term, which amounts to roughly 1/6 of the direct coupling term (A4).

For $n = 2, 3$, and 4 channels and for $\mathcal{I} = 6, 10$, and 20 ru, we have calculated the differences between the eigenvalues of the matrix $-\mathbf{M}(x)$ and the analytical results for $n = 2$. These differences have been least-squares fitted to a series of the form \mathcal{I}^{q-2}/x^q and $q \geq 4$. The coefficients are always very small. The difference between the $n = 3$ and $n = 2$ cases is even smaller and between the $n = 4$ and $n = 3$ results it is almost negligible. This rapid stabilization of the adiabatic representation as the number of channels increases reflects the tridiagonal structure of the Hamiltonian matrix, with off-diagonal terms $\Delta\ell = \pm 2$.

4. Asymptotic behavior of $\mathcal{M}(x_{\text{max}})$: Numerical calculations

Here we analyze the influence of the asymptotic BCs for the inward integration at x_{max} given in Sec. 1 and of the number of coupled channels on the field-dressed scattering length. For $n = 2, 3$, and 4 channels, i.e., $\ell = 0, 2$, $\ell = 0, 2, 4$, and $\ell = 0, 2, 4, 6$, respectively, we have performed a large number of numerical calculations in the interval $0.142\,152 \text{ ru} \leq x_{00} \leq 0.152\,135 \text{ ru}$, which corresponds to the field-free scattering length varying from $-\infty$ to $+\infty$. Remember that each value of x_{00} is associated with a specific pair of atoms.

In the multichannel asymptotic boundary conditions labeled BC2 (BC26) in Table V, we have used the pairs of functions BC2 (BC26) of Table III for any ℓ . For the BC24 conditions, the BC24 functions were used in the $\ell = 0$ channel and either the BC2 or BC26 pairs in the other channels, both leading to the same results. For $v_{p=4}^{\ell=0}(x)$, we have considered either the adiabatic s -wave potential of the two-channel model (A4) with $c_4 = 2\mathcal{I}^2/135$ or this term plus the nonadiabatic contri-

TABLE V. First three coefficients of the expansion of $\mathcal{M}(x_{\max})$ in powers of $1/x_{\max}$ obtained by a fit performed with x_{\max} spanning the interval [20 ru, 500 ru], with different asymptotic boundary conditions [column 2, labeled BC and related to the potential V_f given in column 3 (see the Appendix, Sec. 1)] and three different nonresonant field intensities \mathcal{I} (column 1), using three coupled channels ($\ell = 0, 2$, and 4). The calculations were performed using 150 or 200 values of x_{00} [Eq. (13)] chosen such that the field-free s -wave scattering length varies from $-\infty$ to $+\infty$. The table reflects the dependence on x_{00} of these coefficients: Either they are constant (coefficient of $1/x_{\max}$, column 5) or they present a characteristic shape (see Fig. 4) with three divergences (constant coefficient, column 4, and coefficient of $1/x_{\max}^2$, column 6). The constant coefficient $\mathcal{M}_0(\mathcal{I}, x_{00})$ varies with x_{00} and \mathcal{I} , but not with the BCs and is equal to the field-dressed scattering length $\tilde{a}(\mathcal{I}, x_{00})$ [Eq. (17)]. Its particular value for $x_{00} = 0.148\,741$ ru [i.e., $\tilde{a}(\mathcal{I} = 0) = 0.786\,619$ ru] is given in parentheses in column 4, to show the precision of its determination by the fit. For each value of \mathcal{I} and for each type of initial condition, the variation with x_{00} of the coefficient of $1/x_{\max}^2$, labeled $\eta(\mathcal{I}, x_{00})$ in column 6, depends on the boundary conditions (which is expressed by the different superscripts) but exhibits always a shape very similar to the one of $\tilde{a}(\mathcal{I}, x_{00})$; more precisely, it is related to \mathcal{M}_0 by a linear transformation [Eq. (A6)]. Column 7 shows the dependence on \mathcal{I} of the coefficient of $1/x_{\max}$.

\mathcal{I} (ru)	Label	$V_f(x)$	Constant coefficient	Coefficient of $1/x_{\max}$	Coefficient of $1/x_{\max}^2$	Coefficient of \mathcal{I}^2/x_{\max}
6	BC2	0	$\tilde{a}(\mathcal{I}, x_{00})$ (0.105964)	0.64002	$\eta(\mathcal{I}, x_{00})$	0.017778
6	BC26	$-1/x^6$	$\tilde{a}(\mathcal{I}, x_{00})$ (0.105964)	0.64002	$\eta'(\mathcal{I}, x_{00})$	0.017778
6	BC24	$-c_4/x^4$	$\tilde{a}(\mathcal{I}, x_{00})$ (0.105964)	0.1067	$\eta''(\mathcal{I}, x_{00})$	0.002964
6	BC24*	$-c_4^*/x^4$	$\tilde{a}(\mathcal{I}, x_{00})$ (0.105964)	0.01781	$\eta^{**}(\mathcal{I}, x_{00})$	0.0004947
10	BC2	0	$\tilde{a}(\mathcal{I}, x_{00})$ (-3.28493)	1.7779	$\eta(\mathcal{I}, x_{00})$	0.017779
10	BC26	$-1/x^6$	$\tilde{a}(\mathcal{I}, x_{00})$ (-3.28492)	1.778	$\eta'(\mathcal{I}, x_{00})$	0.01778
10	BC24	$-c_4/x^4$	$\tilde{a}(\mathcal{I}, x_{00})$ (-3.28492)	0.2962	$\eta''(\mathcal{I}, x_{00})$	0.002962
10	BC24*	$-c_4^*/x^4$	$\tilde{a}(\mathcal{I}, x_{00})$ (-3.28493)	0.0495	$\eta^{**}(\mathcal{I}, x_{00})$	0.000495
20	BC2	0	$\tilde{a}(\mathcal{I}, x_{00})$ (-1.77085)	7.1125	$\eta(\mathcal{I}, x_{00})$	0.017781
20	BC26	$-1/x^6$	$\tilde{a}(\mathcal{I}, x_{00})$ (-1.77086)	7.112	$\eta'(\mathcal{I}, x_{00})$	0.01778
20	BC24	$-c_4/x^4$	$\tilde{a}(\mathcal{I}, x_{00})$ (-1.77086)	1.186	$\eta''(\mathcal{I}, x_{00})$	0.002965
20	BC24*	$-c_4^*/x^4$	$\tilde{a}(\mathcal{I}, x_{00})$ (-1.77085)	0.198	$\eta^{**}(\mathcal{I}, x_{00})$	0.000495

bution (A5) with $c_4^* = 7\mathcal{I}^2/405$. These two cases are referred to as BC24 and BC24*, respectively.

For each x_{00} , we have calculated $\mathcal{M}(x_{\max})$ for $20 \text{ ru} \leq x_{\max} \leq 500 \text{ ru}$, using the method described in Sec. III B. A fitting of $\mathcal{M}(x_{\max})$ to a polynomial in $1/x_{\max}$ provides the first coefficients of the expansion of $\mathcal{M}(x_{\max})$ in powers of $1/x_{\max}$. In this way, we obtain the dependence of these coefficients on x_{00} . The results for three coupled channels, i.e., $\ell = 0, 2$, and 4, are presented in Table V for $\mathcal{I} = 6, 10$, and 20 ru. The coefficients are either x_{00} independent (coefficient of $1/x_{\max}$, column 5) or they present a characteristic shape (see Fig. 4)

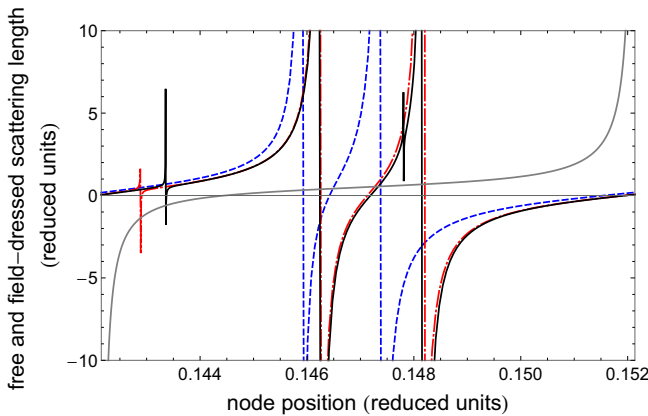


FIG. 4. Field-dressed s -wave scattering length for $n = 2$ (blue dashed line), $n = 3$ (red dot-dashed line), and $n = 4$ (black solid line) channels and $\mathcal{I} = 10$ ru. The field-free scattering length (gray line) is also plotted.

with several (three, in the results of Table V, where we consider three channels) divergences (constant coefficient, column 4, and coefficient of $1/x_{\max}^2$, column 6), the position in x_{00} of the divergences only depending on \mathcal{I} and on the number of channels.

The constant term \mathcal{M}_0 , which is the field-dressed scattering length $\tilde{a}(\mathcal{I}, x_{00})$, only depends on \mathcal{I} and on x_{00} , i.e., on the field intensity and on the atom pair, but not on the boundary conditions. The accuracy of this procedure is illustrated by values of the field-dressed scattering length for the specific choice of $x_{00} = 0.148\,741$ ru [i.e., $\tilde{a}(\mathcal{I} = 0) = 0.786\,619$ ru] (see values in parentheses in the fourth column of Table V): A dependence on the boundary condition appears at most in the sixth digit.

The coefficient of $1/x_{\max}$ is independent of x_{00} , but depends on the boundary conditions and is proportional to \mathcal{I}^2 (see columns 5 and 7 of Table V). The coefficients of \mathcal{I}^2/x_{\max} are identical for BC2 and BC26 (0.017 78), smaller for BC24 (0.002 96), and even smaller for BC24* (0.000 49). These differences are due to the way the term $1/x^4$ is considered in the boundary conditions of the s wave.

To compare with the analytical results of Table IV, we examine the coefficients of the \mathcal{I}^2/x_{\max} factor in the $\mathcal{M}(x_{\max})$ expansion (column 7 of Table V). We first recall that an approximation for the s -wave field-dressed potential is $-c_4^*/x^4$, a sum of the adiabatic and nonadiabatic two-channel contributions (A5). With the boundary conditions BC2 and BC26, which do not include a $1/x^4$ term, the coefficient of \mathcal{I}^2/x_{\max} is close to $c_4^* = 0.017\,28$, as expected. When the direct coupling term proportional to $1/x^4$ between the $\ell = 0$ and $\ell = 2$ channels is included in the reference functions, the cor-

responding contribution disappears in the \mathcal{I}^2/x_{\max} coefficient of the $\mathcal{M}(x_{\max})$ expansion: This explains why the difference between the boundary conditions BC2 and BC24 is 0.01482 or $\approx 2/135$. Analogously, a comparison of the BC24 and BC24* results shows that when the nonadiabatic couplings are accounted for, the \mathcal{I}^2/x_{\max} coefficient in the $\mathcal{M}(x_{\max})$ expansion decreases by $0.00247 \approx 1/405$. These multichannel results testing the influence of the asymptotic boundary conditions on the \mathcal{I}^2/x_{\max} coefficient agree perfectly with the single-channel two-potential model. The small but nonvanishing coefficient of $1/x_{\max}$ in the BC24* case provides an estimate for the differences between the single-channel analytical approach, which includes the adiabatic plus nonadiabatic contributions, and the multichannel model with a full numerical calculation. The BC24* boundary condition yields the smallest coefficient of the $1/x_{\max}$ term in $\mathcal{M}(x_{\max})$ (see Table V), which is approximately equal to $0.198/20 \sim 0.01$ ru for $\mathcal{I} = 20$ ru and $x_{\max} = 20$ ru. This value gives an estimate of the error introduced in the field-dressed scattering length when the dependence of $\mathcal{M}(x_{\max})$ on x_{\max} is neglected and when the field-dressed scattering length is set equal to $\mathcal{M}(x_{\max})$ instead of \mathcal{M}_0 . The boundary conditions BC24* thus represent the best choice to systematically calculate the field-dressed scattering length.

The coefficient of $1/x_{\max}^2$ in the numerical expansion of $\mathcal{M}(x_{\max})$, labeled $\eta(\mathcal{I}, x_{00})$ (see column 6 of Table V), depends on \mathcal{I} and on x_{00} and have a dependence on x_{00} similar to the one of $\mathcal{M}_0(\mathcal{I}, x_{00}) = \tilde{a}(\mathcal{I}, x_{00})$. One has

$$\eta(\mathcal{I}, x_{00}) = m_2 \tilde{a}(\mathcal{I}, x_{00}) + m_1, \quad (\text{A6})$$

with coefficients depending both on \mathcal{I} and on the boundary conditions. The two-potential model predicts also a linear

transformation, with coefficients depending on the reference functions and on the coefficients c_4 , c_{4f} , and c_5 (see Table IV). We find that the slope m_2 is proportional to \mathcal{I}^2 and the additional constant m_1 to \mathcal{I}^3 . This could be expected from the analytical results of Table IV and from the adiabatic potential (A4) and the nonadiabatic coupling term (A5), whose $1/x^4$ and $1/x^5$ terms vary as \mathcal{I}^2 and \mathcal{I}^3 , respectively.

The field-dressed scattering length as a function of x_{00} is presented in Fig. 4 for $\mathcal{I} = 10$ ru, comparing $n = 2, 3$, and 4 channels. The considered range of x_{00} corresponds to one quasiperiod of the field-free scattering length, i.e., the latter, which is also plotted (in gray), varies once over the whole domain $[-\infty, +\infty]$. When increasing n by one unit, an additional divergence appears, related to the new channel with a larger ℓ . While the poles with $\tilde{\ell} = 0$ and $\tilde{\ell} = 2$ are difficult to distinguish, because the coupling between these two channels is very large at this intensity, it is easy to identify the $\tilde{\ell} \geq 4$ value of the field-dressed channel associated with a particular divergence and to see how the position of these divergences changes with increasing n . The location of the poles with $\tilde{\ell} = 0$ and $\tilde{\ell} = 2$ are approximately stabilized as soon as the $\ell = 4$ and $\ell = 6$ channels are introduced in the model. Indeed, the field-dressed scattering length reaches an almost stable value in the three-channel model, except for divergences related to shape resonances with $\tilde{\ell} \geq 4$. The width of the poles, as x_{00} is varied, is large for $\tilde{\ell} = 0$ and 2 and becomes narrower as $\tilde{\ell}$ increases. By fixing x_{00} and varying \mathcal{I} , the width of the poles as a function of intensity decreases rapidly as $\tilde{\ell}$ increases (see Figs. 1 and 2). In this range of intensity, a control of the scattering length could only use the $\tilde{\ell} = 0$ and 2 divergences.

-
- [1] A. Derevianko, *Phys. Rev. A* **67**, 033607 (2003).
[2] Z. Idziaszek and T. Calarco, *Phys. Rev. Lett.* **96**, 013201 (2006).
[3] J. Dalibard, in *Proceedings of the International School of Physics "Enrico Fermi," Course CXL*, Varenna, 1998, edited by M. Inguscio, S. Stringari, and C. E. Wieman (IOS, Amsterdam, 1999), Vol. 140, pp. 321–349.
[4] S. Giorgini, L. P. Pitaevskii, and S. Stringari, *Rev. Mod. Phys.* **80**, 1215 (2008).
[5] C. Chin, R. Grimm, P. Julienne, and E. Tiesinga, *Rev. Mod. Phys.* **82**, 1225 (2010).
[6] M. Theis, G. Thalhammer, K. Winkler, M. Hellwig, G. Ruff, R. Grimm, and J. H. Denschlag, *Phys. Rev. Lett.* **93**, 123001 (2004).
[7] S. Blatt, T. L. Nicholson, B. J. Bloom, J. R. Williams, J. W. Thomsen, P. S. Julienne, and J. Ye, *Phys. Rev. Lett.* **107**, 073202 (2011).
[8] R. Yamazaki, S. Taie, S. Sugawa, K. Enomoto, and Y. Takahashi, *Phys. Rev. A* **87**, 010704 (2013).
[9] M. Yan, B. J. DeSalvo, B. Ramachandhran, H. Pu, and T. C. Killian, *Phys. Rev. Lett.* **110**, 123201 (2013).
[10] P. O. Fedichev, Y. Kagan, G. V. Shlyapnikov, and J. T. M. Walraven, *Phys. Rev. Lett.* **77**, 2913 (1996).
[11] J. L. Bohn and P. S. Julienne, *Phys. Rev. A* **56**, 1486 (1997).
[12] V. Kokouline, J. Vala, and R. Kosloff, *J. Chem. Phys.* **114**, 3046 (2001).
[13] R. Ciuryło, E. Tiesinga, and P. S. Julienne, *Phys. Rev. A* **71**, 030701 (2005).
[14] R. González-Férez and C. P. Koch, *Phys. Rev. A* **86**, 063420 (2012).
[15] M. Tomza, R. González-Férez, C. P. Koch, and R. Moszynski, *Phys. Rev. Lett.* **112**, 113201 (2014).
[16] B. Gao, *Phys. Rev. A* **58**, 4222 (1998).
[17] B. Gao, *Phys. Rev. A* **64**, 010701 (2001).
[18] B. Gao, *J. Phys. B* **36**, 2111 (2003).
[19] A. Crubellier and E. Luc-Koenig, *J. Phys. B* **39**, 1417 (2006).
[20] B. Gao, *Phys. Rev. A* **80**, 012702 (2009).
[21] B. E. Londoño, J. E. Mahecha, E. Luc-Koenig, and A. Crubellier, *Phys. Rev. A* **82**, 012510 (2010).
[22] A. Crubellier, R. González-Férez, C. P. Koch, and E. Luc-Koenig, *New J. Phys.* **17**, 045020 (2015).
[23] A. Crubellier, R. González-Férez, C. P. Koch, and E. Luc-Koenig, *New J. Phys.* **17**, 045022 (2015).
[24] M. Marinescu and L. You, *Phys. Rev. Lett.* **81**, 4596 (1998).
[25] V. Roudnev and M. Cavagnero, *J. Phys. B* **42**, 044017 (2009).
[26] J. L. Bohn, M. Cavagnero, and C. Ticknor, *New J. Phys.* **11**, 055039 (2009).

- [27] T. F. O'Malley, L. Spruch, and L. Rosenberg, *J. Math. Phys.* **2**, 491 (1961).
- [28] B. Deb and L. You, *Phys. Rev. A* **64**, 022717 (2001).
- [29] A. Crubellier, O. Dulieu, F. Masnou-Seeuws, M. Elbs, H. Knöckel, and E. Tiemann, *Eur. Phys. J. D* **6**, 211 (1999).
- [30] B. Pasquiou, G. Bismut, Q. Beaufils, A. Crubellier, E. Maréchal, P. Pedri, L. Vernac, O. Gorceix, and B. Laburthe-Tolra, *Phys. Rev. A* **81**, 042716 (2010).
- [31] B. R. Levy and J. B. Keller, *J. Math. Phys.* **4**, 54 (1963).
- [32] L. Silberstein, *Philos. Mag.* **33**, 92 (1917).
- [33] L. Silberstein, *Philos. Mag.* **33**, 215 (1917).
- [34] L. Silberstein, *Philos. Mag.* **33**, 521 (1917).
- [35] M. Lepers, R. Vexiau, M. Aymar, N. Bouloufa-Maafa, and O. Dulieu, *Phys. Rev. A* **88**, 032709 (2013).
- [36] N. Vanhaecke, C. Lisdat, B. T'Jampens, D. Comparat, A. Crubellier, and P. Pillet, *Eur. Phys. J. D* **28**, 351 (2004).
- [37] H. Friedrich, *Theoretical Atomic Physics*, 2nd ed. (Springer, Berlin, 1998).
- [38] L. Landau and E. Lifchitz, *Mécanique Quantique* (Mir, Moscow, 1967).
- [39] O. Hinckelmann and L. Spruch, *Phys. Rev. A* **3**, 642 (1971).
- [40] V. Roudnev and M. Cavagnero, *Phys. Rev. A* **79**, 014701 (2009).
- [41] N. Vanhaecke, Ph.D. thesis, Université Paris XI, 2003.
- [42] B. Gao, *Eur. Phys. J. D* **31**, 283 (2004).
- [43] R. Grimm, M. Weidemüller, and Y. B. Ovchinnikov, *Adv. At. Mol. Opt. Phys.* **42**, 95 (2000).
- [44] A. Crubellier and E. Luc-Koenig (unpublished).
- [45] M. J. Moritz, C. Eltschka, and H. Friedrich, *Phys. Rev. A* **63**, 042102 (2001).
- [46] T. F. O'Malley, *Phys. Rev.* **134**, A1188 (1964).
- [47] R. Shakeshaft, *J. Phys. B* **5**, L115 (1972).